

1 **BrGDGTs-based seasonal paleotemperature reconstruction for the last 15,000 years**  
2 **from a shallow lake on the eastern Tibetan Plateau**

3 Xiaohuan Hou <sup>a</sup>, Nannan Wang <sup>a</sup>, Zhe Sun <sup>b</sup>, Kan Yuan <sup>a, c</sup>, Xianyong Cao <sup>a</sup>, Juzhi Hou <sup>a\*</sup>

4 <sup>a</sup> *Group of Alpine Paleocology and Human Adaptation (ALPHA), State Key Laboratory of Tibetan*  
5 *Plateau Earth System, Resources and Environment (TPESRE), Institute of Tibetan Plateau Research,*  
6 *Chinese Academy of Sciences, Beijing 100101, China*

7 <sup>b</sup> *Institute of Geography and Resources Science, Sichuan Normal University, Chengdu, 610066, China*

8 <sup>c</sup> *University of Chinese Academy of Sciences, Beijing 100049, China*

9

10 \* Corresponding author

11 E-mail address: houjz@itpcas.ac.cn

12

13 **ABSTRACT**

14 Knowledge of Holocene temperature changes is crucial for addressing the problem of the  
15 discrepancy between Holocene proxy temperature reconstructions and climate model  
16 simulations. The complex spatiotemporal pattern of temperature variations on the Tibetan  
17 Plateau (TP) further complicates the study of Holocene continental climate change. The  
18 discrepancy between model-based and proxy-based Holocene temperature reconstructions  
19 possibly results from the seasonal biases and environmental ambiguities of the proxies.  
20 Quantitative temperature reconstructions using different proxies from the same sediment core  
21 can provide an effective means of evaluating different proxies; however, this approach is  
22 unusual in terrestrial environments. Here, we present an ice-free-season temperature record  
23 for the past 15 ka from a shallow, freshwater lake on the eastern TP, based on brGDGTs  
24 (branched glycerol dialkyl glycerol tetraethers). This record shows that the Holocene Thermal  
25 Maximum lags the pollen-based July temperature recorded in the same sediment core. We  
26 conclude that the mismatch between the brGDGTs-based and pollen-based temperatures is  
27 primarily the result of seasonal variations in solar irradiance. The overall pattern of  
28 temperature changes is supported by other summer temperature records, and the Younger  
29 Dryas cold event and the Bølling–Allerød warm period are also detected. A generally warm  
30 period occurred during 8–3.5 ka, followed by cooling in the late Holocene. Our findings have  
31 implications for understanding the seasonal signal of brGDGTs in shallow lakes, and provide  
32 critical data for confirming the occurrence of seasonal biases in different proxies from high-  
33 elevation lakes. To further investigate the significance of the brGDGTs and temperature  
34 patterns on the TP, we reviewed previously published brGDGTs-based Holocene temperature

35 records across the TP. In these studies, brGDGTs have been interpreted to reflect either mean  
36 annual air temperature or growing season temperature. In both cases, brGDGTs reflect a  
37 gradual warming trend during the Holocene with relatively cooler conditions during the  
38 middle Holocene, and a cooling trend during the middle to late Holocene. We analyzed the  
39 possible reasons for the diverse brGDGTs records on the TP and emphasize the importance of  
40 considering lake conditions and modern investigations of brGDGTs in lacustrine systems  
41 when using brGDGTs to reconstruct paleoenvironmental conditions.

42 **Keywords:** Tibetan Plateau, brGDGTs, the mean temperature of Months Above Freezing,  
43 shallow lake, Holocene

## 44 **1 Introduction**

45 Global climate change has had a profound impact on both the natural ecological and socio-  
46 economic systems that are vital for human survival and development, making climate change  
47 a critical limiting factor for the sustainable development of human society. The Tibetan  
48 Plateau (TP), also called the “Third Pole” (Qiu, 2008), has undergone a more rapid warming  
49 over the last five decades, with a rate twice that of the global average (0.3 – 0.4°C/decade)  
50 (Kuang and Jiao, 2016; Chen et al., 2015), making it one of the world's most temperature-  
51 sensitive regions (Chen et al., 2015; Yao et al., 2022). Consequently, assessing the impact of  
52 future climate change on the TP is becoming increasingly important. To enhance the  
53 precision and accuracy of future climate change estimates for the TP under ongoing global  
54 climate change and to minimize the uncertainty in climate simulations, it is essential to  
55 investigate the processes and mechanisms of regional climate and environmental changes,  
56 with particular emphasis on temperature, on a relatively long timescale, such as that of the

57 Holocene.

58

59 The Holocene, the most recent geological epoch, is closely linked with the development of  
60 human civilization. Quantitative reconstructions of Holocene temperature trends can be used  
61 to explore their impacts on civilization and to establish a geological and historical context for  
62 predicting future climate changes. In recent decades, many Holocene quantitative  
63 reconstructions of seasonal and annual temperatures for the TP have been produced using  
64 various proxies, like pollen (Herzschuh et al., 2014; Lu et al., 2011), chironomids (Zhang et  
65 al., 2017; Zhang et al., 2019a),  $\delta^{18}\text{O}$  in ice cores (Pang et al., 2020; Thompson et al., 1997),  
66 and biomarkers (Hou et al., 2016; Zhao et al., 2013; Cheung et al., 2017). These  
67 reconstructions have provided crucial data for the elucidation of Holocene temperature  
68 changes. However, the available Holocene temperature records from the TP show divergent  
69 trends. Multiple proxy indicators indicate three different Holocene temperature patterns on  
70 the TP. First, a consistent Holocene warming trend (Sun et al., 2022; Feng et al., 2022; Opitz  
71 et al., 2015). For example, brGDGTs based annual temperatures (Feng et al., 2022; Sun et al.,  
72 2022) indicate a gradual warming trend which resembles the  $\delta^{18}\text{O}$  temperature record from  
73 the Chongce ice core on the western TP, except for the last 2 ka (Pang et al., 2020). Second,  
74 an early to middle Holocene summer temperature maximum and a gradual cooling trend  
75 during the late Holocene are observed in pollen-, alkenone- and chironomid-based  
76 temperature records (Herzschuh et al., 2014; Hou et al., 2016; Zhang et al., 2017; Wang et al.,  
77 2021a; Zheng et al., 2015). Third, a prominent relatively cool middle Holocene (Wang et al.,  
78 2021c; Li et al., 2017); for example, a composite temperature record suggests that  
79 temperatures were  $\sim 2^\circ\text{C}$  cooler during the middle Holocene than during the early and late

80 Holocene (Wang et al., 2021c). Several records also show a steady long-term trend without  
81 distinct cooling or warming (Sun et al., 2021). Moreover, the cooling trends in proxy-based  
82 Holocene temperature records are inconsistent with those of climate models, which indicate a  
83 warming trend, and this inconsistency is widely known as the “Holocene temperature  
84 conundrum” (Liu et al., 2014). There are several potential factors that may contribute to the  
85 disparity in Holocene temperature trends, including seasonal biases and uncertainties in  
86 temperature proxies and reconstructions, independent of climate models (Liu et al., 2014;  
87 Hou et al., 2019; Bova et al., 2021; Cartapanis et al., 2022; Marsicek et al., 2018). While  
88 several recent studies have suggested that seasonality in proxies is not the major cause of the  
89 Holocene temperature conundrum (Dong et al., 2022; Zhang et al., 2022b), it is significant  
90 that the TP is an alpine and high-altitude region with significant seasonal temperature  
91 variations. Moreover, most organisms tend to grow during the warmer seasons at high  
92 latitudes and high altitudes (Zhao et al., 2021a). Currently, however, we lack unambiguous  
93 and reliable seasonal temperature records to support a seasonality-bias hypothesis. Extensive  
94 research has been conducted in lakes, employing a single proxy to reconstruct past  
95 temperature fluctuations. However, there have been scarce studies that employ various  
96 proxies within the same core to reconstruct paleotemperature variations. Furthermore, the  
97 limited number of studies primarily concentrate on reconstructing summer temperature and  
98 annual average temperature. For example, a chironomid-based July temperature  
99 reconstruction for Tiancai lake on the southeastern TP shows higher temperatures during the  
100 early to middle Holocene (Zhang et al., 2017), while the brGDGTs-based annual average  
101 temperature shows a warming trend (Feng et al., 2022). Different proxies may reflect the

102 seasonal temperatures in different months, and thus producing temperature reconstructions  
103 for different months for the same sediment core may help better understand the seasonal bias  
104 of terrestrial temperature records. Furthermore, the reconciliation of the divergent trends of  
105 Holocene temperature on the TP and its surroundings requires additional high-altitude  
106 temperature records from these regions, with reliable chronologies and proxy records with an  
107 unambiguous climatological significance.

108

109 Branched glycerol dialkyl glycerol tetraethers (brGDGTs) are a group of membrane-spanning  
110 lipids found in bacteria (Fig. S1) (Chen et al., 2022; Halamka et al., 2022; Sinninghe Damsté  
111 et al., 2000), and they have become a powerful tool for quantifying past terrestrial  
112 temperature variations. Through investigations of brGDGTs in globally-distributed soils, it  
113 was found that the distribution of brGDGTs is primarily related to temperature and pH  
114 (Weijers et al., 2007). Subsequently, brGDGTs–temperature calibrations from soil, peat and  
115 lake sediments were established on scales from global (Weijers et al., 2007; De Jonge et al.,  
116 2014; Crampton-Flood et al., 2020; Martínez-Sosa et al., 2021) to regional (e.g., East Asia)  
117 (Sun et al., 2011; Ding et al., 2015; Wang et al., 2016; Dang et al., 2018), leading to  
118 considerable progress in reconstructing terrestrial temperatures, particularly on the TP  
119 (Cheung et al., 2017; Zhang et al., 2022a; Li et al., 2017).

120

121 Natural lakes are widely distributed across the TP (Zhang et al., 2019b). Lake sediments,  
122 characterized by their organic matter-rich composition, exhibit continuous and rapid  
123 accumulation rates. As a result, they offer high-resolution records of environmental changes,

124 making them highly valued as a primary terrestrial climate archive (Moser et al., 2019).  
125 BrGDGTs in lacustrine systems are often more strongly correlated with temperature, with  
126 higher coefficient of determination ( $r^2$ ) and lower root mean square error (RMSE) values  
127 (Martínez-Sosa et al., 2021), than in soils and peats. Nevertheless, the factors that impact the  
128 distribution of brGDGTs in lakes are intricate and multidimensional. Notably, the sources of  
129 brGDGTs within lakes are intricate, involving contributions from soil as well as  
130 autochthonous lake processes. However, an expanding body of research underscores a  
131 substantial prevalence of autochthonous brGDGTs in lakes (Tierney and Russell, 2009;  
132 Tierney et al., 2010; Weber et al., 2015; Wang et al., 2021b). Furthermore, the origins of  
133 brGDGT producers remain uncertain and could be influenced by various factors, including  
134 lake salinity (Wang et al., 2021b), redox conditions (Weber et al., 2018), oxygen content  
135 and/or mixing patterns (Van Bree et al., 2020; Wu et al., 2021; Buckles et al., 2014).  
136 Additionally, even lake depth plays a role due to distinct ecological niches (Woltering et al.,  
137 2012), thereby contributing to the intricate interplay that shapes the distribution of brGDGTs  
138 within lakes.

139

140 In this study, we obtained a quantitative temperature reconstruction for the past 15 ka from  
141 Gahai, a shallow (average depth of ~2 m) freshwater lake located in the source area of the  
142 Yellow River. This region is an important ecological protection area on the eastern edge of  
143 the TP. Freshwater environments avoid the confounding effects of salinity on brGDGTs-  
144 based temperature reconstructions, and shallow lakes also minimize the impact of the uneven  
145 distribution of light and nutrients on brGDGTs. Our specific aims were: (1) to determine the

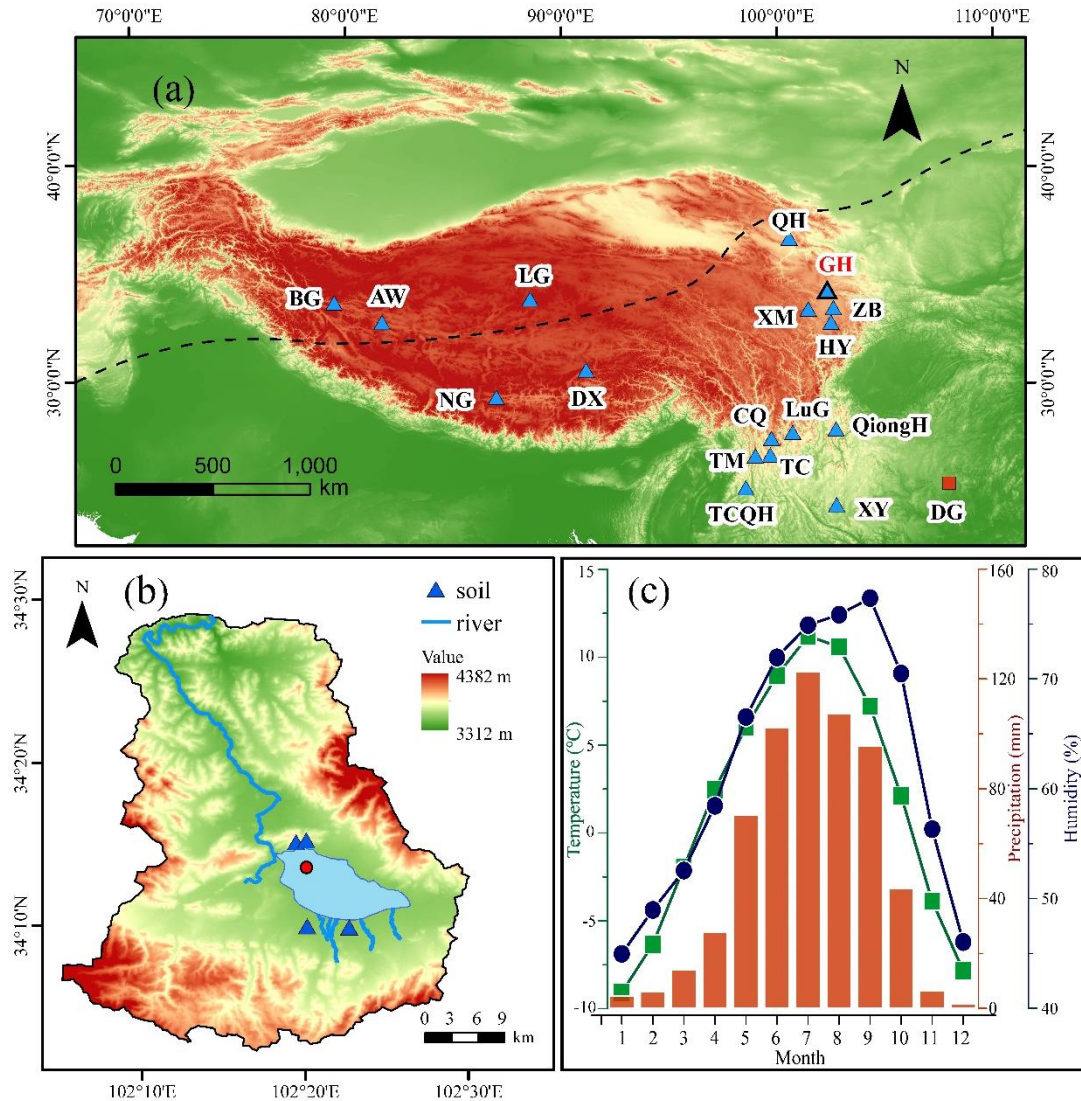
146 long-term trend of Holocene warm-biased terrestrial temperatures at a high elevation; (2) to  
147 compare records of ice-free season temperatures with July temperatures from the same  
148 sediment core; and (3) to gain a better understanding of the possible mechanisms responsible  
149 for Holocene temperature variations, especially on the TP.

## 150 **2 Materials and methods**

### 151 *2.1 Study site*

152 Gahai (102°11'–102°28' E, 34°04'–34°4' N, 3444 m a.s.l.) is a freshwater lake and part of the  
153 Gahai meadow wetland, which is a national nature reserve with restricted human access, on  
154 the eastern edge of the Tibetan Plateau (Fig. 1). The lake is fed by runoff from the  
155 surrounding hills, drains into the Tao River, and ultimately enters the Yellow River. Thus,  
156 Gahai lake is a critical water conservation area in the upper reaches of the Yellow River. The  
157 average water depth of Gahai is ~1–2 m, and the maximum depth is ~5 m. The vegetation in  
158 the catchment consists mainly of *Kobresia tibetica*, *Equisetum arvense*, *Potentilla anserina*,  
159 *Artemisia subulate*, and *Oxytropis falcata* (Ma et al., 2019). Meteorological data for the area  
160 are available from Langmu Temple station (1957-1988) (Fig. 1) (102°38' E, 34°5' N, 3412 m  
161 a.s.l.), ~32 km northwest of Gahai lake. They indicate an annual average (mean) precipitation  
162 of 781 mm, with > 67% occurring between June and September, and mean annual  
163 temperature of 1.2 °C with a relative humidity of ~65%. The summers are mild and humid  
164 and the winters are cold and dry. From May to September, the mean average temperature is  
165 above freezing (0°C), but the temperature in May is very low, close to 0°C.





166

167 **Fig. 1** (a) Locations of the sites on the Tibetan Plateau referenced in the text. Triangle with  
 168 bold line indicates the location of Gahai lake (this study). Other triangles indicate the  
 169 locations of cited studies on the Tibetan Plateau and the surrounding area: Bangong Co  
 170 Co (BG), Aweng Co (AW), Ngamring Co (NG), Linggo Co (LG), Dangxiong wetland (DX),  
 171 Qinghai lake (QH), Ximen Co (XM), Zoige Basin (ZB), Hongyuan peatland (HY), Lugu  
 172 lake (LuG), Cuoqia lake (CQ), Tingming lake (TM), Tengchongqinghai lake (TCQH),  
 173 Tiancai lake (TC), Qionghai lake (QH), Xingyun lake (XY). Red square indicates  
 174 Dongge Cave (DG). Black dotted line represents the northern boundary of the modern  
 175 Asian summer Monsoon (Chen et al., 2008). (b) Drainage basin of Gahai lake and the  
 176 core site. (c) Climate data from Langmu Temple meteorological station: monthly  
 177 temperature (green line), precipitation (red bars), and humidity (blue line).

178 *2.2 Sampling*

179 A sediment core with the length of 329 cm was obtained from Gahai Lake in January 2019, at  
180 a water depth of 1.95 m, using a UWITEC platform operated from the frozen lake surface. In  
181 addition, four catchment soil samples were collected from around the lake (Fig. 1). All  
182 samples were transported to the Institute of Tibetan Plateau Research, Chinese Academy of  
183 Sciences (ITPCAS). The sediment core was split lengthwise, and one half was subsampled  
184 and freeze-dried for subsequent analysis.

185

186 *2.3 Chronology*

187 The chronology of the upper 20 cm of the sediment core is based on measurements of  $^{210}\text{Pb}$   
188 and  $^{137}\text{Cs}$ , at a 1-cm interval. The chronology for the deeper part of the core is provided by  
189 accelerator mass spectrometry (AMS)  $^{14}\text{C}$  measurements of 13 bulk sediment samples, which  
190 were conducted by Beta Analytic Inc. (Miami, USA) (Fig. 2) (Wang et al., 2022).

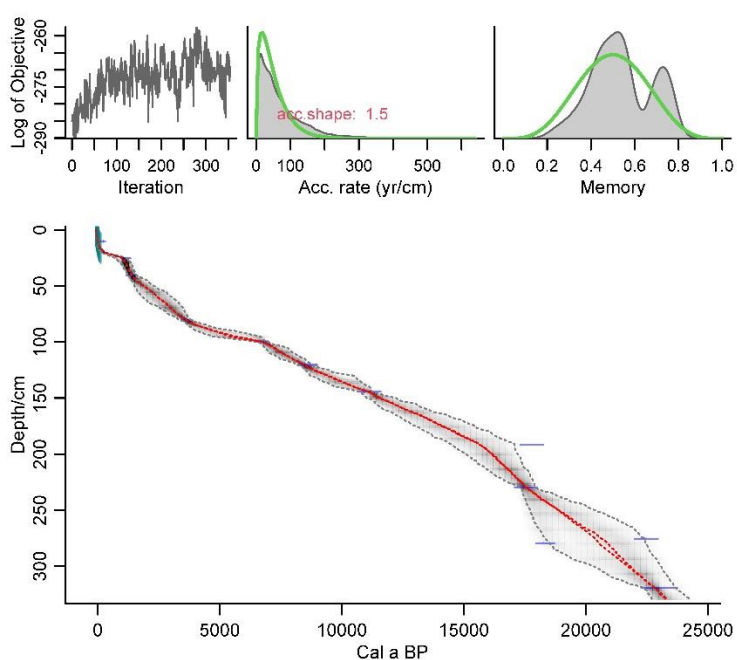
191

192 The  $^{210}\text{Pb}$  age model was constructed using the constant rate of supply (CRS) model and the  
193  $^{137}\text{Cs}$  peak was used as supplement (Appleby, 2002). The calculated age of  $^{210}\text{Pb}$  using CRS  
194 model aligned well with the  $^{137}\text{Cs}$  peak at 6 cm. Overall, the CRS model was deemed suitable  
195 for determining the age of Gahai lake.

196

197 Reservoir age, as highlighted by Hou et al. (2012), is a crucial factor affecting the age  
198 determination of lake sediment cores on the TP. Therefore, it was necessary to establish the  
199 reservoir age of Gahai lake before undertaking paleoclimate reconstruction. The linear

200 extrapolation relationship between the  $^{14}\text{C}$  ages and depth to the sediment-water interface is  
201 often used to estimate the reservoir age. The  $^{14}\text{C}$  age of 13 samples exhibits a good linear  
202 relationship with sediments depth in Gahai lake. Extrapolation of this 13  $^{14}\text{C}$  ages down to the  
203 depth of 6 cm yielded a  $^{14}\text{C}$  age of 461 yr BP, while the reliable  $^{210}\text{Pb}$  age at 6 cm is -27 yr BP.  
204 Consequently, the difference between the two ages, which amounts to 488 yr, was taken as  
205 the reservoir age. Additionally, it's worth noting that independent estimations of the  $^{14}\text{C}$   
206 calibration age and  $^{210}\text{Pb}$  age around 10 cm in Gahai lake was obtained, resulting in values of  
207 497 yr BP and 18 yr BP, respectively. The difference of 479 yr between these two ages can  
208 also be considered as the reservoir age. These two methods of estimating reservoir age of  
209 Gahai lake show very close, which are mutually supportive. So, the average of 483 yr was  
210 adopted as the reservoir age. All original  $^{14}\text{C}$  dates were corrected by subtracting the reservoir  
211 age (483 yr) and calibrating them to calendar ages using Calib 8.1. The age-depth model (Fig.  
212 2) was constructed using the Bacon program with the  $^{14}\text{C}$  ages and  $^{210}\text{Pb}$  ages (Blaauw and  
213 Andres Christen, 2011) and was reported by Wang et al. (2022).



214

215 **Fig. 2** Age-depth model for Gahai, based on AMS  $^{14}\text{C}$ ,  $^{210}\text{Pb}$  and  $^{137}\text{Cs}$  ages (Wang et al.,  
216 2022). The ages of the upper 20 cm are based on  $^{210}\text{Pb}$  and  $^{137}\text{Cs}$  dating (green symbols)  
217 and those of the lower part on AMS  $^{14}\text{C}$  dates (blue symbols).

218

#### 219 *2.4 Lipids extraction and brGDGTs analysis*

220 For lipids extraction, ~5 g samples were ground to a powder and extracted ultrasonically with  
221 dichloromethane (DCM): methanol (MeOH) (9: 1, v: v) three times. The supernatants were  
222 combined and dried under a stream of nitrogen gas. Subsequently, the total lipid extracts were  
223 separated into neutral and acid fractions through a LC-NH<sub>2</sub> silica gel column using DCM:  
224 isopropyl alcohol (2: 1, v: v) and ether with 4% acetic acid (v: v), respectively. The neutral  
225 fraction was then eluted through a silica gel column using n-Hexane, DCM and MeOH, and  
226 the GDGTs were dissolved in the MeOH. The GDGTs fraction was passed through a 0.45  $\mu\text{m}$   
227 polytetrafluoroethylene (PTFE) filter before analysis. C<sub>46</sub>-GDGT (a standard compound)  
228 (Huguet et al., 2006) was added to the samples before analysis.

229

230 BrGDGTs were detected using an HPLC-APCI-MS (Waters ACQUITY UPLC I-Class/Xevo  
231 TQD) with auto-injection at the ITPCAS. The compounds were separated by three Hypersil  
232 Gold Silica LC columns in sequence (each 100 mm  $\times$  2.1 mm, 1.9  $\mu\text{m}$ , Thermo Fisher  
233 Scientific; USA), maintained at a temperature of 40°C. GDGTs were eluted isocratically  
234 using 84% hexane and 16% ethyl acetate (EtOA) for the first 5 min, followed by a linear  
235 gradient change to 82% hexane and 18% EtOA from 5 to 65 min. The columns were cleaned  
236 using 100% EtOA for 10 min, and then back to 84% hexane and 16% EtOA to equilibrate the  
237 column, with a flow rate of 0.2 ml min<sup>-1</sup>.

238

239 The APCI-MS conditions were as follows: nebulizer pressure at 60 psi, APCI probe  
240 temperature at 400°C, drying gas flow rate of 6 L/min and temperature of 200°C, capillary  
241 voltage of 3600 V, source corona of 5.5  $\mu$ A. Detection was performed in selected ion  
242 monitoring (SIM) mode, targeting the protonated molecules at m/z 1050, 1048, 1046, 1036,  
243 1034, 1032, 1022, 1020, 1018 and 744. The results were analyzed using MassLynx V4.1  
244 software, and quantification was achieved by comparing the peak areas of targeted ions and  
245 the internal standard, assuming an identical response factor for GDGTs.

246

### 247 **3 Results and Discussion**

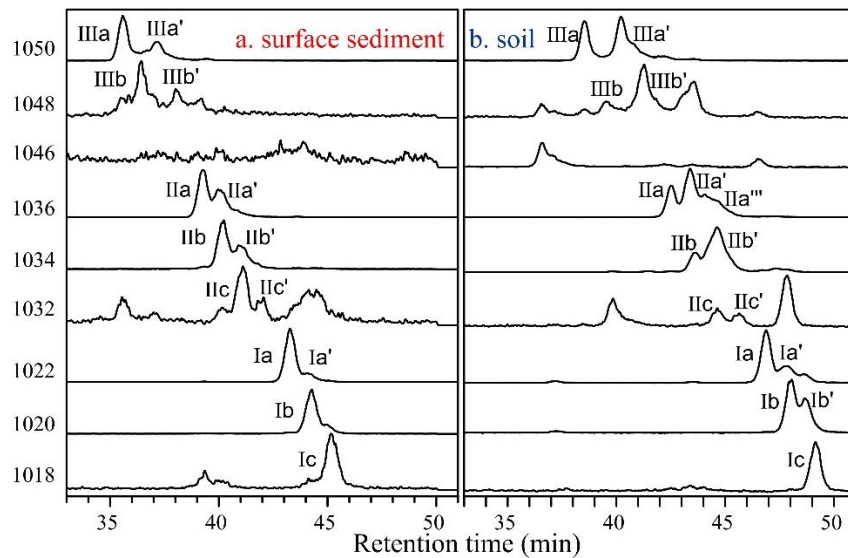
#### 248 *3.1. Concentration and distribution of brGDGTs in the sediment core and catchment soils*

249 BrGDGTs were detected in both the catchment soils and the downcore sediments. The  
250 average concentration of brGDGTs in the catchment soils (0.07 ng g<sup>-1</sup>dw) was lower than in  
251 the surficial core sediments (0.70 ng g<sup>-1</sup>dw). In the soil samples, pentamethylated brGDGTs  
252 were generally the most abundant (55.33%), followed by tetramethylated brGDGTs (23.60%)  
253 and hexamethylated brGDGTs (21.07%) (Fig. S2). The relative amount of cyclopentane ring-  
254 containing brGDGTs in the soil samples was generally low (24.34%) and it was sometimes  
255 too low to be detected, especially the fractions of IIIb, IIIb', IIIc, IIIc', IIc and IIc'. In the  
256 downcore sediments, the relative abundant of tetramethylated brGDGTs (43.84%) was like  
257 that of pentamethylated brGDGTs (41.93%), and hexamethylated brGDGTs were the least  
258 abundant (14.22%) (Fig. S2). The relative abundant of cyclopentane ring-containing  
259 brGDGTs in the downcore sediments (67.82%) was lower than that in the catchment soils.

260 *3.2 In situ production of brGDGTs in Gahai lake*

261 Although lacustrine brGDGTs have great potential for quantitatively reconstructing terrestrial  
262 paleotemperatures, uncertainties about their sources in lacustrine environments are a major  
263 factor limiting their application (Tierney and Russell, 2009; Cao et al., 2020; Sun et al., 2011;  
264 Sinninghe Damsté et al., 2009; Buckles et al., 2014). To investigate the origin and  
265 characteristics of brGDGTs in the Gahai lake sediments, we examined the distributions and  
266 concentrations of brGDGTs in the sediments and catchment soils and found notable  
267 differences between them. First, as described in the previous section, the average content of  
268 brGDGTs in the catchment soils was ~10% that of the surficial lake sediments, suggesting the  
269 absence of large-scale allochthonous inputs from the catchment soils. Second, the brGDGTs  
270 distributions in the downcore sediments were quite different from those in the catchment soils,  
271 which suggests a substantial autochthonous brGDGTs contribution to the lake sediments (Fig.  
272 3 and Fig. S2). Moreover, the ratios of 6-methyl brGDGTs to 5-methyl GDGTs ( $IR_{6ME}$ ) in the  
273 soils and sediments, calculated according to the formula proposed by De Jonge et al. (2014),  
274 were different. In the soil samples,  $IR_{6ME}$  varied between 0.54 and 0.57 and the average ratio  
275 in the downcore samples was 0.26, varying between 0.18 and 0.47. Third, the in-situ  
276 production of brGDGTs in Gahai lake is suggested by the discrepancies in the degree of  
277 methylation ( $MBT'_{5ME}$ ) between the soils and surface sediments. The average value of  
278  $MBT'_{5ME}$  in the Gahai lake surface sediments was 0.48, which is clearly higher than in the  
279 catchment soils, with the range of 0.32–0.35. Fourth, and potentially the most significant, the  
280 IIIb' and Ib' compounds are present in the catchments soil but not in the Gahai lake surficial  
281 sediments, which may be direct evidence of an autochthonous brGDGTs contribution in the

282 lacustrine environment (Fig. 3), and a lower proportion of soil-derived brGDGTs input.  
283 Therefore, we conclude that the brGDGTs in the Gahai lake sediments are mainly of in-situ  
284 origin.



285

286 **Fig. 3** Representative high-performance liquid chromatography/atmospheric pressure  
287 chemical ionization-mass spectrometry (HPLC/APCIMS) chromatograms of brGDGTs  
288 from (a) surface sediments from Gahai lake, and (b) soils in the catchment of Gahai lake.

289

### 290 3.3 brGDGTs-temperature calibration and Holocene temperature reconstruction

291 Gahai is a shallow lake in the eastern Tibetan Plateau that is typically completely frozen  
292 during winter and spring. Local meteorological data indicate that the average snowfall period  
293 lasts for 269 days, with around 50 days of continuous snowfall (Luqu County Local  
294 Chronicles Compilation Committee, 2006). The freezing of the lake surface begins in late  
295 October each year and gradually thaws starting from May of the following year. As a result,  
296 the light transmittance and oxygen content in the lake water are reduced during the freezing  
297 season, leading to decreased nutrient levels, which severely hinder the growth of autotrophic

298 microorganisms. Although the bacteria responsible for producing brGDGTs have not been  
299 thoroughly characterized, the abundance of heterotrophic bacteria will likely decrease due to  
300 the reduced autotrophic biomass during the winter and spring ice-covered period. The  
301 weakened light penetration, decreased oxygen levels, and lack of nutrient replenishment  
302 during the frozen period significantly impact the growth of autochthonous microorganisms.

303

304 Furthermore, some research suggests that the production of brGDGTs might be related to  
305 factors such as water depth, seasonal alternation of water column mixing and stratification  
306 (Loomis et al., 2014; Van Bree et al., 2020). During the summer and autumn seasons when  
307 the lake ice melts and the water becomes more mobile, the nutrient content increases,  
308 resulting in elevated lake biomass, moreover, the oxygen levels at the bottom of Gahai lake  
309 are not expected to be too high, which could further contribute to the proliferation of  
310 brGDGT-producing bacteria, potentially leading to an increase in the brGDGT-producing  
311 bacteria (Weber et al., 2018). Therefore, brGDGTs in Gahai lake may provide records of the  
312 average temperature during the ice-free months of the summer and autumn seasons.

313

314 Additionally, the presence of the frozen lake surface during winter creates a thermal barrier,  
315 impeding the exchange of heat between the lake water and the atmosphere. Consequently,  
316 any brGDGTs generated within the lake water during this period lose their ability to  
317 accurately reflect atmospheric temperature variations (Sun et al., 2021; Zhang et al., 2022a).  
318 Thus, they were no longer able to track atmospheric temperature changes during the frozen  
319 season. So, we prefer to use Gahai brGDGTs to reconstruct temperatures during the summer



320 and ice-free seasons. For this purpose, we employed the new Bayesian calibration for the  
321 mean temperature of the Months Above Freezing (MAF), as proposed by Martínez-Sosa et al.  
322 (2021), to derive a MAF for Gahai lake.

323

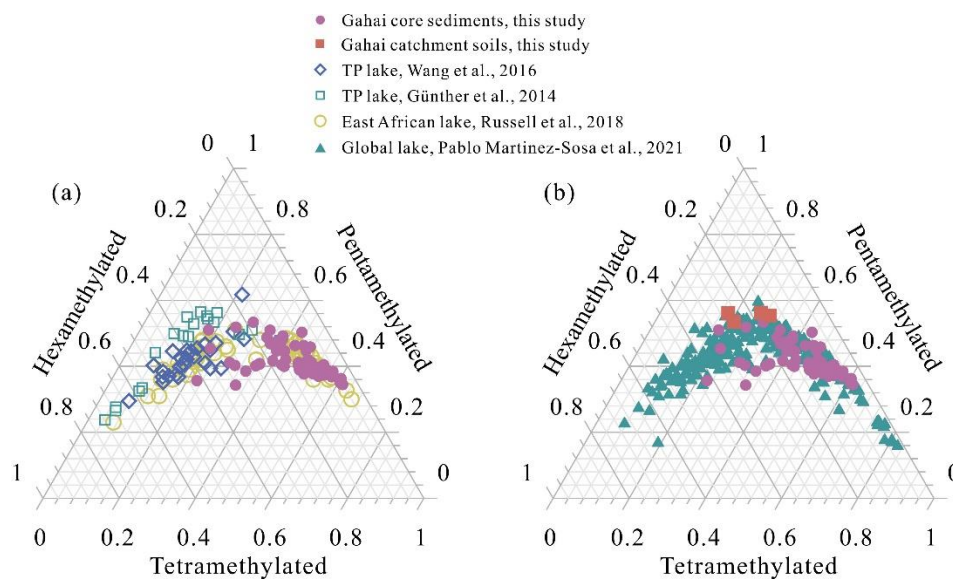
324 To assess the accuracy of this calibration approach, we compared the fractional abundances  
325 of summed tetra-, penta-, and hexamethylated brGDGTs in Gahai lake sediments with other  
326 datasets (Fig. 4). These datasets include lake sediments from the Tibetan Plateau (Günther et  
327 al., 2014; Wang et al., 2016), East Africa (Russell et al., 2018), and global lakes (Martínez-  
328 Sosa et al., 2021). The distribution pattern of Gahai core sediments is distinctly remarkable  
329 compared to that of other lake sediments within the Tibetan Plateau, even though they share a  
330 common regional origin (Fig. 4). However, its resemblance to the global distribution of  
331 brGDGTs in lake sediments is evident. Notably, the calibration developed by Martínez-Sosa  
332 et al. (2021) is based on brGDGTs from a global lake dataset.

333

334 Using calibration of Martínez-Sosa's et al. (2021), we reconstructed the surface sediment  
335 temperature of Gahai lake, resulting in a temperature estimate of 9.4°C. This reconstructed  
336 temperature closely matches the ice-free season temperature recorded by meteorological  
337 stations in the Gahai region (8.8°C for May to September). Furthermore, considering the  
338 significant contribution of autochthonous brGDGTs in Gahai lake, we also attempted to  
339 reconstruct the Holocene paleotemperature record using previously published lake-specific  
340 brGDGTs-temperature calibrations (e.g., Günther et al., 2014; Martínez-Sosa et al., 2021;  
341 Russell et al., 2018; Sun et al., 2011; Wang et al., 2016). As depicted in Fig. S3, most of these

342 calibrations exhibit qualitatively similar temperature change patterns when applied to the  
343 sediment core from Gahai Lake. This similarity arises from their shared same principles, just  
344 utilizing distinct datasets, resulting in records that display analogous trends but vary in  
345 absolute temperatures.

346



347

348 **Fig. 4** Comparison of the fractional abundances of tetramethylated, pentamethylated, and  
349 hexamethylated bGDGTs in sediment core samples from Gahai with lake surface  
350 sediments from the Tibetan Plateau (Wang et al., 2016; Günther et al., 2014), East Africa  
351 (Russell et al., 2018), and worldwide (Martínez-Sosa et al., 2021).

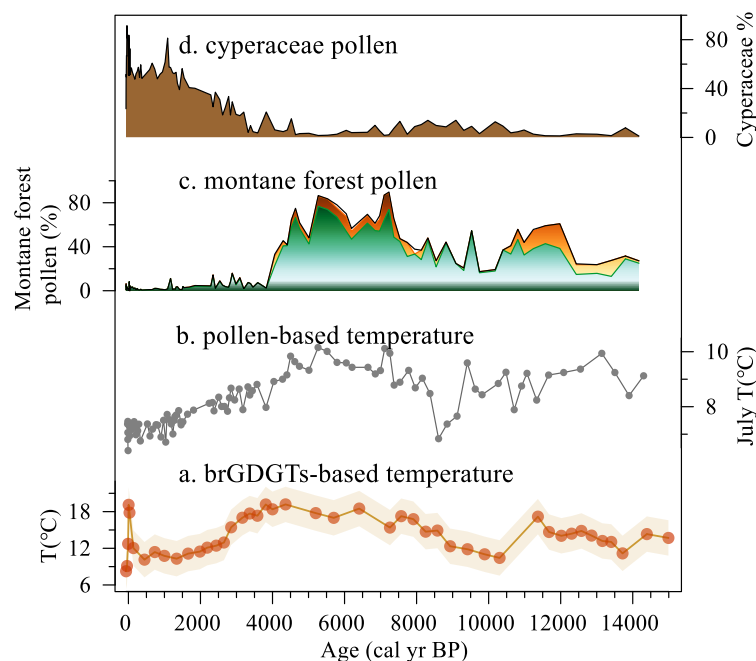
352

353 The depth interval of 191–279 cm in the Gahai sediment core represents an interval of rapid  
354 allocthonous sedimentation, or alternatively a slump, and therefore the results for the  
355 corresponding time interval of 20–15 ka may be unreliable. Thus, our temperature record of  
356 Months Above Freezing from the eastern TP spans the past 15 ka, with the average  
357 temperature of 4°C, as shown in Fig. 5a. Within the range of age uncertainties, weak warming  
358 occurred during 14.8–11.8 ka, likely to corresponding to the Bølling–Allerød (B/A)

359 interstadial. A minor cold reversal occurred during 11.8–10.5 ka, potentially corresponding to  
360 the Younger Dryas (YD) event. Notably, the samples collected between 11.8 ka and 10.5 ka  
361 exhibited GDGT concentrations below the detection limit. Therefore, we directly linked the  
362 temperature reconstructions at the two aforementioned time points, ~11.8 ka and ~10.5 ka,  
363 resulting in the lowest temperature of this time period appearing around 10.5 ka. This may  
364 cause a time lag with the occurrence of the YD event. The temperature record indicates a  
365 colder period during 11.5–8.0 ka. During 8.0–3.5 ka, Gahai experienced a stable warm period  
366 with the average temperature of ~16.5°C, after which the temperature decreased gradually.  
367 Overall, the maximum temperature difference since 15 ka was ~10°C. As for the absolute  
368 temperature changes since 15,000 yr, although some influential studies indicate a warming of  
369 approximately 6.1–7°C from the deglaciation onset to preindustrial times (Tierney et al., 2020;  
370 Osman et al., 2021). However, these results are based on global mean sea surface  
371 temperatures. Our reconstructed temperature range is about 10°C, considering the remarkable  
372 ‘elevation-dependent warming’ observed in high-altitude regions compared to low-altitude  
373 areas (Mountain Initiative EDW Working Group, 2015). Thus, this range could be accurate.  
374 Nevertheless, we do not rule out the possibility that our temperature reconstruction may  
375 exhibit an overestimation. Aside from potential uncertainties associated with the biomarkers  
376 themselves, calibrations may also considerably influence the observed amplitude. We  
377 examined temperature variations reconstructed using different calibrations (Fig. S3), with the  
378 smallest range being 6°C and the largest being 12°C. Undoubtedly, further efforts are needed  
379 to constrain the inherent uncertainties related to biomarker-based temperature reconstructions.  
380

381 3.4 Holocene temperature changes on the eastern edge of TP and their origin

382 Despite the difference in amplitude, the temperature record of Months Above Freezing from  
383 Gahai resembles the pollen record and the pollen-based temperature reconstruction from the  
384 same site (Fig. 5) (Wang et al., 2022). However, the brGDGTs-based Holocene Thermal  
385 Maximum (HTM) lags the pollen-based reconstruction (Fig. 5a, b). Wang et al. (2022) used a  
386 weighted-averaging partial least regression approach to produce a temperature record for  
387 Gahai, based on a modern pollen dataset (n=731) from the eastern TP. Assessment of the  
388 statistical significance of the pollen-based climate variables for Gahai suggests that the mean  
389 July temperature is the most important environmental factor influencing the fossil pollen  
390 assemblages. The brGDGTs in Gahai are indicative of summer and autumn temperatures, and  
391 the mismatch between the temperature records inferred from brGDGTs and the pollen record  
392 may be attributed to the difference between the solar irradiance during June–October and that  
393 during July. A detailed analysis of this topic will be undertaken in the subsequent section.



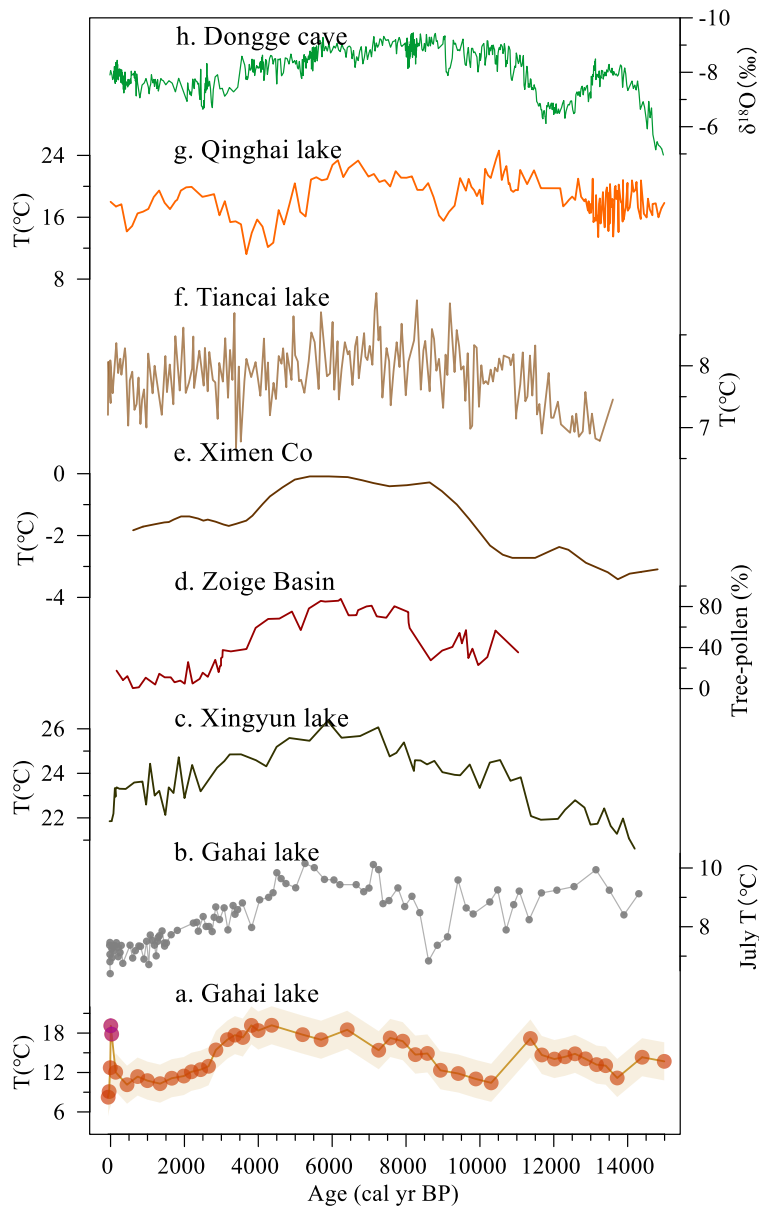
394

395 **Fig. 5** Comparison of multiproxy records from Gahai lake. (a) brGDGTs-based MAF (this

396 study). (b) Temperature of the warmest month (July) based on pollen assemblages  
397 (Wang et al., 2022). (c, d) Pollen-reconstructed montane forest (*Pinus*, *Picea*, *Abies*) and  
398 Cyperaceae pollen record (Wang et al., 2022).

399

400 The brGDGTs-based temperature record from Gahai confirms the occurrence of a climate  
401 optimum in the mid-Holocene on the northeast Tibetan Plateau, which is consistent with  
402 several other pollen and pollen-reconstructed temperature records from the fringe areas of the  
403 Asian summer monsoon (Fig. 6), suggesting that it is a reliable representation of Holocene  
404 temperature changes in this region. For example, pollen-based temperature reconstructions  
405 from Xingyun lake and Ximen Co on the eastern TP show a early to middle HTM (9–4 ka)  
406 and a cooling trend thereafter (Fig. 6c, e) (Wu et al., 2018; Herzschuh et al., 2014; Wang et  
407 al., 2021a). Additionally, lake water temperature reconstructions based on subfossil  
408 chironomids from Tiancai lake (Fig. 6f) (Zhang et al., 2017; Zhang et al., 2019a) and  
409 alkenones from Qinghai lake (Fig. 6g) (Hou et al., 2016) show the same trends during the  
410 past 15 ka, as also shown by other pollen-based temperature records from the TP (Chen et al.,  
411 2020). Pollen, chironomids and alkenones mainly respond to the growing season  
412 temperatures in middle and high latitudes, and thus the reconstructed temperature records are  
413 consistent with the variations in summer solar irradiance. Similar variations were documented  
414 in temperature reconstructions at a global scale (Marcott et al., 2013; Cartapanis et al., 2022).



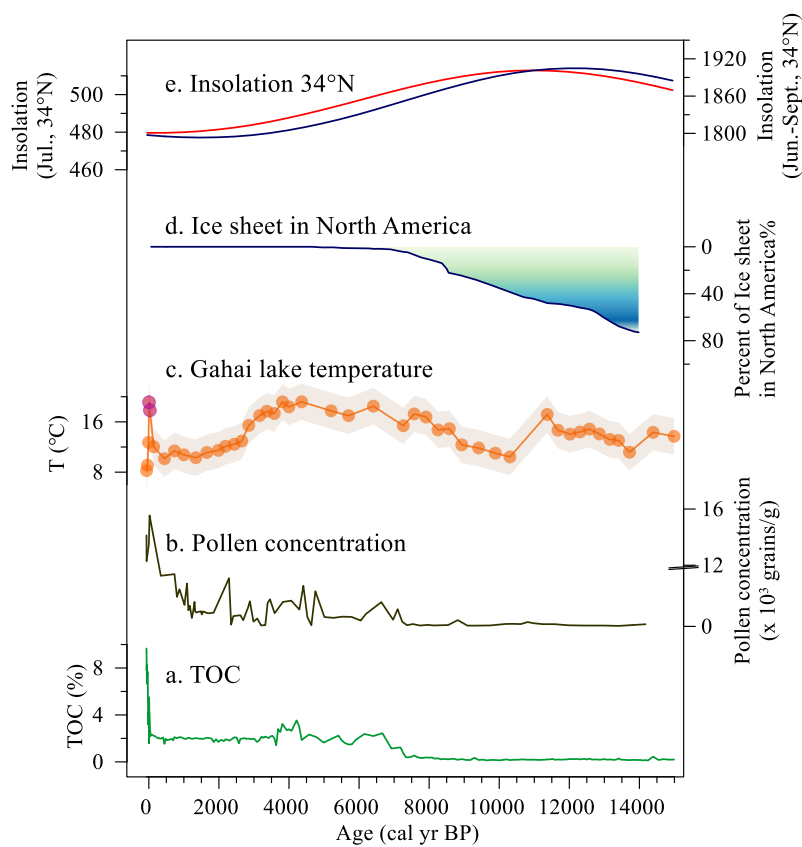
415

416 **Fig. 6** Comparison of temperature at Gahai and other records from the eastern edge of the  
 417 Tibetan Plateau. (a) brGDGTs-based MAF at Gahai, the purple dots may indicate  
 418 unreliable temperature changes influenced by human activities (this study). (b)  
 419 Temperature of the warmest month (July) based on pollen data from Gahai (Wang et al.,  
 420 2022). (c) Pollen-based temperature at Xingyun lake (Wu et al., 2018). (d) Tree pollen  
 421 percentages from the Hongyuan peatland in the southern Zoige Basin (Zhou et al., 2010).  
 422 (e) Pollen-based temperature at Ximen Co (Herzschuh et al., 2014). (f) Chironomid-  
 423 based temperature at Tiancai lake (Zhang et al., 2017, 2019a). (g) Alkenone-based  
 424 temperature at Qinghai lake (Hou et al., 2016). (h) Stalagmite  $\delta^{18}\text{O}$  record of Donge  
 425 cave (Dykoski et al., 2005).

426

427 Nevertheless, the timing and amplitude of the Gahai temperature fluctuations differ from  
428 those of other temperature records from this region (Fig. 6). These discrepancies may be the  
429 result of the chronological uncertainties of these records, and to differences in the seasonal  
430 and spatial responses to climate forcing and feedbacks. The temperature records shown in Fig.


431 6 mostly refer to summer temperatures, which are primarily influenced by summer insolation.



432

433 **Fig. 7** Temperature fluctuations and forcing factors during the Holocene. (a, b) TOC content  
434 and pollen concentrations from Gahai (Wang et al., 2022). (c) brGDGTs-based MAF  
435 from Gahai, the purple dots may indicate unreliable temperature changes influenced by  
436 human activities (this study). (d) Percentage of the remnant Laurentide ice sheet in  
437 North America relative to the Last Glacial Maximum (Dyke, 2004). (e) Local insolation  
438 at 34 °N during ice-free months (Laskar et al., 2004).

439

440 The temperature record in Gahai during the early Holocene fails to closely track the Northern  
441 Hemisphere insolation trend, and there is also a time lag. The pollen-based temperature  
442 record for Xingyun Lake in southwestern China also shows lower temperatures in the early  
443 Holocene (Fig. 6c). The albedo effect caused by the increased cloud cover may be the reason  
444 for the early Holocene decrease in summer temperatures (Wu et al., 2018). However, the  
445 pollen record from Gahai indicates dry conditions during the early Holocene (Wang et al.,  
446 2022), and cloud cover may not be the primary factor responsible for the low temperatures at  
447 this time. The melting of Northern Hemisphere ice sheets during the early Holocene  
448 weakened the Atlantic Meridional Overturning Circulation (AMOC) and potentially also the  
449 global thermohaline circulation. This led to a reduction in the amount of heat transport by the   
450 North Atlantic warm current to high-latitude regions, which resulted in the low temperatures  
451 in middle to high latitudes of the Northern Hemisphere. The persistence of the Laurentide ice  
452 sheet into the early Holocene maintained the regional albedo, as well as discharging  
453 meltwater into the North Atlantic (Fig. 7d) (Dyke, 2004). In addition, a Holocene temperature  
454 simulation showed that global warming was more pronounced when dust factors were  
455 excluded from the simulation (Liu et al. (2018)). The record of insoluble particles in the  
456 Greenland GISP2 ice core indicates relatively high concentrations of atmospheric aerosols in  
457 the early Holocene (Zielinski and Mershon, 1997), which would have weakened summer  
458 solar irradiation via radiative feedback, leading to the cool temperatures during this period.  
459 These factors may together have caused the early Holocene temperature decline at Gahai  
460 Lake, which slightly delayed the onset of the Holocene Warm Period.



461

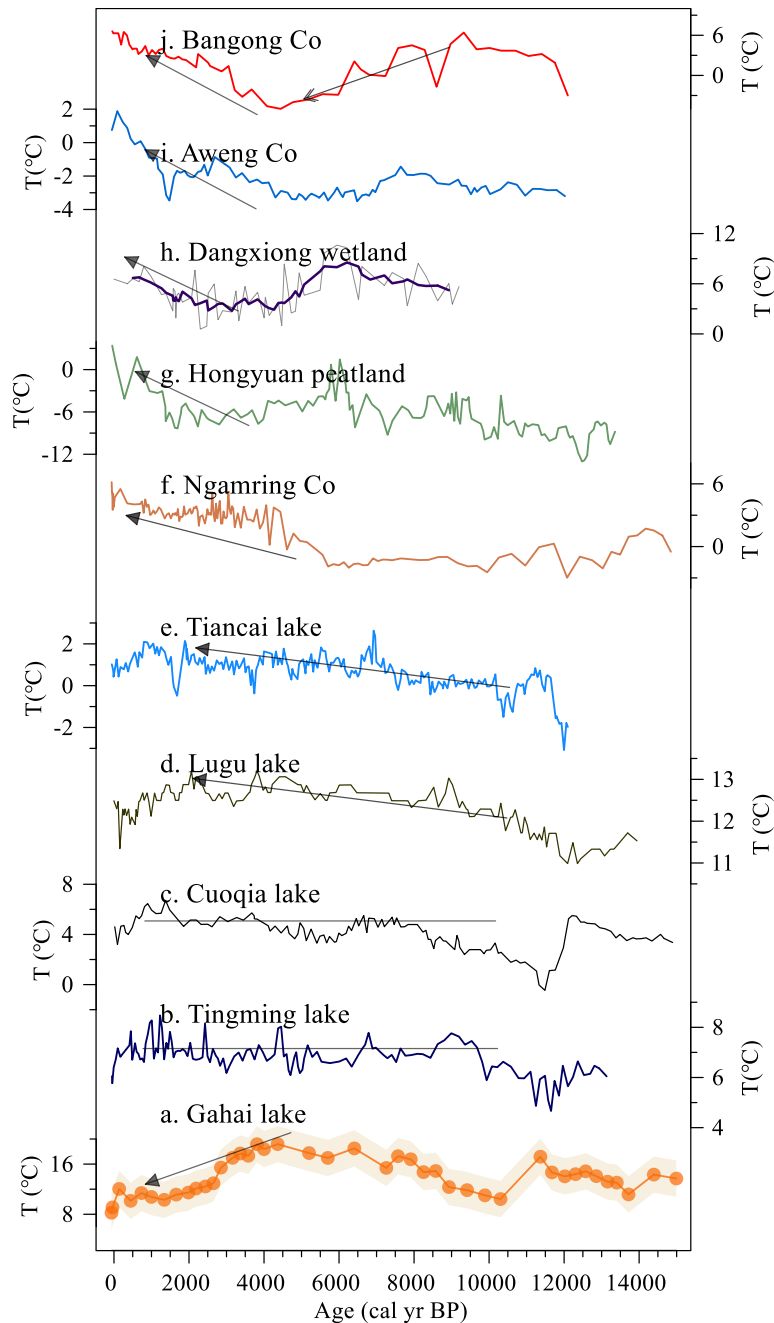
462 A notable and rapid temperature increase is evident at Gahai in recent decades, which differs  
463 from the other records (Fig. 7c). Moreover, there are notable increases in pollen concentration,  
464 TOC, and TN (Fig. 7a, b) in the Gahai sediment core, indicating intensive local human  
465 activities like grazing and tourism, which may be the primary cause of the environmental  
466 changes in this region (Wang et al., 2022). This intensive human activity may have reduced  
467 the ability of the brGDGTs to record the natural temperature background. These observations  
468 emphasize the important impact of human activities on climate proxies and the need to  
469 carefully consider their effect on temperature reconstructions.

470

### 471 *3.5 Spatiotemporal pattern of brGDGTs-based TP temperatures*

472 In addition to comparing the Gahai temperature with the summer temperature records from  
473 the eastern TP and its surrounding areas, we compiled and reviewed published Holocene  
474 brGDGTs-based quantitative temperature records from across the TP. As shown in Fig. 8,  
475 with the increasing number of these records for the TP, the differences between the results  
476 have become more pronounced. The brGDGTs records from lakes in the central and western  
477 parts of the plateau show higher temperatures in the early and late Holocene, and lower  
478 temperatures in the middle Holocene (Wang et al., 2021c; Li et al., 2017; He et al., 2020),  
479 while the brGDGTs records from lakes in the southern and south-eastern parts of the TP show  
480 a warming trend throughout the Holocene (Sun et al., 2022; Feng et al., 2022). In addition,  
481 brGDGTs in Cuoqia lake and Tingming lake, on the south-eastern TP, recorded the ice-free  
482 season temperature, which was relatively stable during the Holocene (Sun et al., 2021; Zhang

483 et al., 2022a). However, our temperature record from Gahai is different from the above  
 484 records and resembles summer temperature changes during the Holocene (Chen et al., 2020).  
 485 This is because the brGDGTs record from Lake Gahai represents warm season temperatures,  
 486 which adds to its reliability.



487  
 488 **Fig. 8** Comparison of Holocene temperature based on brGDGTs at Gahai (a) and other  
 489 records from around the TP. Reconstructed ice-free-season temperatures from (b)

490 Tingming lake (Sun et al., 2021), (c) Cuoqia lake (Zhang et al., 2022a). Reconstructed  
491 annual temperature from (d) Lugu lake (Zhao et al., 2021b), (e) Tiancai lake (Feng et al.,  
492 2022), (f) Ngamring Co(Sun et al., 2022), (g) Hongyuan peatland (Yan et al., 2021). (h)  
493 Dangxiong wetland (Cheung et al., 2017), (i) Aweng Co (Li et al., 2017), (j) Bangong  
494 Co (Wang et al., 2021c).

495


496 We suggest that the complexity of Holocene temperature patterns recorded by brGDGTs in  
497 TP lakes is primarily due to the ambiguity of brGDGTs in these lakes, as well as to the spatial  
498 heterogeneity of climate change across the TP. This ambiguity can be attributed to several  
499 factors. First, the origin of brGDGTs in lakes remains an uncertain factor in temperature  
500 reconstruction. An increasing number of studies indicate the occurrence of a remarkable  
501 amount of autochthonous brGDGTs in lakes, but their abundance in soil can also affect the  
502 distribution of brGDGTs in lakes due to their supply via soil erosion (e.g., Tierney and  
503 Russell, 2009; Weber et al., 2015; Wang et al., 2023). In fact, even within the same lake (e.g.,  
504 Tengchongqinghai lake in southwestern China), two studies reached inconsistent conclusions  
505 regarding the origin of brGDGTs (Tian et al., 2019; Zhao et al., 2021b), possibly because the  
506 niches of certain brGDGTs may expand or contract compared to other locations within a lake.  
507 Therefore, it is important to conduct detailed modern process studies to accurately assess the  
508 sources of brGDGTs in lakes, especially with regard to evaluating the proportion of  
509 autochthonous brGDGTs (Wang et al., 2023; Martin et al., 2020). Second, brGDGTs may  
510 show a seasonal signal. Current brGDGTs–temperature calibrations for lakes reflect the  
511 annual average temperature (Sun et al., 2011; De Jonge et al., 2014), as well as the growing

512 season temperature (Sun et al., 2011; Dang et al., 2018) and the ice-free season temperature  
513 (Martínez-Sosa et al., 2021; Zhang et al., 2022a). Thus, there is no consensus regarding  
514 whether the brGDGTs have a seasonal bias, and it is necessary to conduct continuous, high-  
515 resolution seasonal investigations of lakes on the Tibetan Plateau to comprehensively  
516 elucidate the seasonal characteristics of brGDGTs. This can enhance the accuracy of regional  
517 temperature reconstruction and may help reconcile the complex temperature patterns  
518 observed on the Tibetan Plateau. Third, the factors affecting the distribution of brGDGTs in  
519 lakes are complex, including not only temperature, pH and salinity but also oxygen content,  
520 water depth, and so on (Wang et al., 2021b; Wang et al., 2016). The distribution of brGDGTs  
521 in lakes is significantly influenced by the hydrological and physical properties of the lakes,  
522 and thus it is necessary to attain a more comprehensive understanding of the characteristics of  
523 the lakes in the study area and their effects on brGDGTs. Fourth, different brGDGTs–  
524 temperature calibrations may lead to markable differences in both the amplitude and trend of  
525 temperature from the same dataset (Wang et al., 2016; Feng et al., 2019). One reason for this  
526 is the deviation between in-situ measured temperature and atmospheric temperature (Wang et  
527 al., 2020). Thus, selecting an appropriate calibration and attempting to establish a brGDGTs-  
528 in situ temperature calibration are effective means of enhancing the reliability of brGDGTs-  
529 based temperature reconstructions.

530

#### 531 **4 Conclusions**

532 We present a quantitative, brGDGTs-based seasonal paleotemperature record over the last 15  
533 ka from the sediments of a shallow lake on the eastern Tibetan Plateau. Our reconstruction


534 resembles the summer temperature trend, with the Holocene Thermal Maximum occurring  
535 during 8–3.5 ka. There is a lag between our brGDGTs-based reconstruction and pollen-based   
536 July temperature recorded in the same sediment core, indicating a seasonal bias between  
537 different proxies. Since 3.5 ka, the temperature decreased gradually, and the surficial  
538 sediments reliably recorded the warm season temperature during the current period in the  
539 Gahai Lake region. However, intensive local human activity during the last century has  
540 affected the distribution of brGDGTs, resulting in temperature deviations recorded by  
541 brGDGTs. However, the implementation of environmental protection policies have reduced  
542 this anthropogenic signal. Our findings help better understand the seasonal signal of  
543 brGDGTs in shallow lakes and provide important data for improving projections of terrestrial  
544 climate change at high elevations.

545

546 We also investigated previously published brGDGTs-based Holocene temperature records on  
547 the TP to determine the pattern of brGDGTs-based temperature changes and the possible  
548 causes of the differences between reconstructions. We emphasize the need for the careful  
549 examination of both the source and behavior of these compounds in lacustrine environments  
550 and lake status, prior to the application of brGDGTs proxies in paleolimnological  
551 reconstruction.

552

### 553 **Data availability**

554 The data used in this study can be obtained from the corresponding author Juzhi Hou  
555 (houjz@itpcas.ac.cn). 

556

557 **Author contributions**

558 Xiaohuan Hou did the experiments, analyzed the data and wrote the manuscript. Nannan  
559 Wang, Zhe Sun, Kan Yuan and Xianyong Cao participated in sample collecting and data  
560 analysis. Juzhi Hou designed this study and led the interpretation. All authors commented on  
561 and improved the manuscript.

562

563 **Competing interests**

564 The contact author has declared that none of the authors has any competing interests.

565

566 **Acknowledgements**

567 This work was financially supported by the National Natural Science Foundation of China  
568 (42025103, 41877459) and the Second Tibetan Plateau Scientific Expedition and Research  
569 (2019QZKK0601). We would like to thank Jan Bloemendal for the help with language  
570 editing.

571

572 **References**

573

574 Bova, S., Rosenthal, Y., Liu, Z., Godad, S. P., and Yan, M.: Seasonal origin of the thermal  
575 maxima at the Holocene and the last interglacial, *Nature*, 589, 548-553, 10.1038/s41586-020-  
576 03155-x, 2021.

577 Buckles, L. K., Weijers, J. W. H., Verschuren, D., and Damste, J. S. S.: Sources of core and  
578 intact branched tetraether membrane lipids in the lacustrine environment: Anatomy of Lake  
579 Challa and its catchment, equatorial East Africa, *Geochimica Et Cosmochimica Acta*, 140,  
580 106-126, 10.1016/j.gca.2014.04.042, 2014.

581 Cao, J., Rao, Z., Shi, F., and Jia, G.: Ice formation on lake surfaces in winter causes warm-  
582 season bias of lacustrine brGDGT temperature estimates, *Biogeosciences*, 17, 2521-2536,  
583 10.5194/bg-17-2521-2020, 2020.

584 Cartapanis, O., Jonkers, L., Moffa-Sanchez, P., Jaccard, S. L., and de Vernal, A.: Complex  
585 spatio-temporal structure of the Holocene Thermal Maximum, *Nat Commun*, 13, 5662,  
586 10.1038/s41467-022-33362-1, 2022.

587 Chen, D., Xu, B., Yao, T., Guo, Z., Cui, P., Chen, F., Zhang, R., Zhang, X., Zhang, Y., Fan, J.,  
588 Hou, Z., and Zhang, T.: Assessment of past, present and future environmental changes on the  
589 Tibetan Plateau, *Chinese Science Bulletin*, 60, 3025-3035, 2015.

590 Chen, F., Yu, Z., Yang, M., Ito, E., Wang, S., Madsen, D. B., Huang, X., Zhao, Y., Sato, T.,  
591 Birks, H. J. B., Boomer, I., Chen, J., An, C., and Wünnemann, B.: Holocene moisture  
592 evolution in arid central Asia and its out-of-phase relationship with Asian monsoon history,  
593 *Quaternary Science Reviews*, 27, 351-364, 10.1016/j.quascirev.2007.10.017, 2008.

594 Chen, F., Zhang, J., Liu, J., Cao, X., Hou, J., Zhu, L., Xu, X., Liu, X., Wang, M., Wu, D.,  
595 Huang, L., Zeng, T., Zhang, S., Huang, W., Zhang, X., and Yang, K.: Climate change,  
596 vegetation history, and landscape responses on the Tibetan Plateau during the Holocene: A  
597 comprehensive review, *Quaternary Science Reviews*, 243, 10.1016/j.quascirev.2020.106444,  
598 2020.

599 Chen, Y., Zheng, F., Yang, H., Yang, W., Wu, R., Liu, X., Liang, H., Chen, H., Pei, H., Zhang,  
600 C., Pancost, R. D., and Zeng, Z.: The production of diverse brGDGTs by an Acidobacterium  
601 providing a physiological basis for paleoclimate proxies, *Geochimica et Cosmochimica Acta*,  
602 337, 155-165, 10.1016/j.gca.2022.08.033, 2022.

603 Cheung, M.-C., Zong, Y., Zheng, Z., Liu, Z., and Aitchison, J. C.: Holocene temperature and  
604 precipitation variability on the central Tibetan Plateau revealed by multiple palaeo-climatic  
605 proxy records from an alpine wetland sequence, *The Holocene*, 27, 1669-1681,  
606 10.1177/0959683617702225, 2017.

607 Committee, L. C. L. C. C.: *Luqu County Chronicles*, Gansu Cultural Publishing House,  
608 Lanzhou, 71 pp.2006.

609 Crampton-Flood, E. D., Tierney, J. E., Peterse, F., Kirkels, F. M. S. A., and Damste, J. S. S.:  
610 BayMBT: A Bayesian calibration model for branched glycerol dialkyl glycerol tetraethers in  
611 soils and peats, *Geochimica Et Cosmochimica Acta*, 268, 142-159,  
612 10.1016/j.gca.2019.09.043, 2020.

613 Dang, X., Ding, W., Yang, H., Pancost, R. D., Naafs, B. D. A., Xue, J., Lin, X., Lu, J., and  
614 Xie, S.: Different temperature dependence of the bacterial brGDGT isomers in 35 Chinese  
615 lake sediments compared to that in soils, *Organic Geochemistry*, 119, 72-79,

616 10.1016/j.orggeochem.2018.02.008, 2018.

617 De Jonge, C., Hopmans, E. C., Zell, C. I., Kim, J.-H., Schouten, S., and Sinninghe Damsté, J.  
618 S.: Occurrence and abundance of 6-methyl branched glycerol dialkyl glycerol tetraethers in  
619 soils: Implications for palaeoclimate reconstruction, *Geochimica et Cosmochimica Acta*, 141,  
620 97-112, 10.1016/j.gca.2014.06.013, 2014.

621 Ding, S., Xu, Y., Wang, Y., He, Y., Hou, J., Chen, L., and He, J. S.: Distribution of branched  
622 glycerol dialkyl glycerol tetraethers in surface soils of the Qinghai-Tibetan Plateau:  
623 implications of brGDGTs-based proxies in cold and dry regions, *Biogeosciences*, 12, 3141-  
624 3151, 10.5194/bg-12-3141-2015, 2015.

625 Dong, Y., Wu, N., Li, F., Zhang, D., Zhang, Y., Shen, C., and Lu, H.: The Holocene  
626 temperature conundrum answered by mollusk records from East Asia, *Nat Commun*, 13,  
627 5153, 10.1038/s41467-022-32506-7, 2022.

628 Dyke, A. S.: An outline of North American deglaciation with emphasis on central and  
629 northern Canada, *Quaternary Glaciations-Extent and Chronology, Pt 2: North America*, 2,  
630 373-424, 10.1016/s1571-0866(04)80209-4, 2004.

631 Dykoski, C. A., Edwards, R. L., Cheng, H., Yuan, D. X., Cai, Y. J., Zhang, M. L., Lin, Y. S.,  
632 Qing, J. M., An, Z. S., and Revenaugh, J.: A high-resolution, absolute-dated Holocene and  
633 deglacial Asian monsoon record from Dongge Cave, China, *Earth and Planetary Science  
634 Letters*, 233, 71-86, 10.1016/j.epsl.2005.01.036, 2005.

635 Feng, X., Zhao, C., D'Andrea, W. J., Liang, J., Zhou, A., and Shen, J.: Temperature  
636 fluctuations during the Common Era in subtropical southwestern China inferred from  
637 brGDGTs in a remote alpine lake, *Earth and Planetary Science Letters*, 510, 26-36,  
638 10.1016/j.epsl.2018.12.028, 2019.

639 Feng, X., Zhao, C., D'Andrea, W. J., Hou, J., Yang, X., Xiao, X., Shen, J., Duan, Y., and Chen,  
640 F.: Evidence for a Relatively Warm Mid - to Late Holocene on the Southeastern Tibetan  
641 Plateau, *Geophysical Research Letters*, 49, 10.1029/2022gl098740, 2022.

642 Group, M. I. E. W.: Elevation-dependent warming in mountain regions of the world, *Nature  
643 Climate Change*, 5, 424-430, 10.1038/nclimate2563, 2015.

644 Günther, F., Thiele, A., Gleixner, G., Xu, B., Yao, T., and Schouten, S.: Distribution of  
645 bacterial and archaeal ether lipids in soils and surface sediments of Tibetan lakes:  
646 Implications for GDGT-based proxies in saline high mountain lakes, *Organic Geochemistry*,  
647 67, 19-30, 10.1016/j.orggeochem.2013.11.014, 2014.

648 Halamka, T. A., Raberg, J. H., McFarlin, J. M., Younkin, A. D., Mulligan, C., Liu, X. L., and  
649 Kopf, S. H.: Production of diverse brGDGTs by *Acidobacterium Solibacter usitatus* in  
650 response to temperature, pH, and O<sub>2</sub> provides a culturing perspective on brGDGT proxies  
651 and biosynthesis, *Geobiology*, 10.1111/gbi.12525, 2022.

652 He, Y., Hou, J., Wang, M., Li, X., Liang, J., Xie, S., and Jin, Y.: Temperature Variation on the  
653 Central Tibetan Plateau Revealed by Glycerol Dialkyl Glycerol Tetraethers From the  
654 Sediment Record of Lake Linggo Co Since the Last Deglaciation, *Frontiers in Earth Science*,  
655 8, 10.3389/feart.2020.574206, 2020.

656 Herzsuh, U., Borkowski, J., Schewe, J., Mischke, S., and Tian, F.: Moisture-advection  
657 feedback supports strong early-to-mid Holocene monsoon climate on the eastern Tibetan  
658 Plateau as inferred from a pollen-based reconstruction, *Palaeogeography, Palaeoclimatology,  
659 Palaeoecology*, 402, 44-54, 10.1016/j.palaeo.2014.02.022, 2014.



660 Hou, J., Li, C., and Lee, S.: The temperature record of the Holocene: progress and  
661 controversies, *Science Bulletin*, 10.1016/j.scib.2019.02.012, 2019.

662 Hou, J., Huang, Y., Zhao, J., Liu, Z., Colman, S., and An, Z.: Large Holocene summer  
663 temperature oscillations and impact on the peopling of the northeastern Tibetan Plateau,  
664 *Geophysical Research Letters*, 43, 1323-1330, 10.1002/2015gl067317, 2016.

665 Huguët, C., Hopmans, E. C., Febo-Ayala, W., Thompson, D. H., Sinninghe Damsté, J. S., and  
666 Schouten, S.: An improved method to determine the absolute abundance of glycerol  
667 dibiphytanyl glycerol tetraether lipids, *Organic Geochemistry*, 37, 1036-1041,  
668 10.1016/j.orggeochem.2006.05.008, 2006.

669 Kuang, X. and Jiao, J. J.: Review on climate change on the Tibetan Plateau during the last  
670 half century, *Journal of Geophysical Research: Atmospheres*, 121, 3979-4007,  
671 10.1002/2015jd024728, 2016.

672 Laskar, J., Robutel, P., Joutel, F., Gastineau, M., Correia, A. C. M., and Levrard, B.: A long-  
673 term numerical solution for the insolation quantities of the Earth, *Astronomy & Astrophysics*,  
674 428, 261-285, 10.1051/0004-6361:20041335, 2004.

675 Li, X., Wang, M., Zhang, Y., Lei, L., and Hou, J.: Holocene climatic and environmental  
676 change on the western Tibetan Plateau revealed by glycerol dialkyl glycerol tetraethers and  
677 leaf wax deuterium-to-hydrogen ratios at Aweng Co, *Quaternary Research*, 87, 455-467,  
678 10.1017/qua.2017.9, 2017.

679 Liu, Y., Zhang, M., Liu, Z., Xia, Y., Huang, Y., Peng, Y., and Zhu, J.: A Possible Role of Dust  
680 in Resolving the Holocene Temperature Conundrum, *Scientific Reports*, 8, 10.1038/s41598-  
681 018-22841-5, 2018.

682 Liu, Z. Y., Zhu, J., Rosenthal, Y., Zhang, X., Otto-Bliesner, B. L., Timmermann, A., Smith, R.  
683 S., Lohmann, G., Zheng, W. P., and Timm, O. E.: The Holocene temperature conundrum,  
684 *Proc. Natl. Acad. Sci. U. S. A.*, 111, E3501-E3505, 10.1073/pnas.1407229111, 2014.

685 Loomis, S. E., Russell, J. M., Heuroux, A. M., D'Andrea, W. J., and Sinninghe Damsté, J. S.:  
686 Seasonal variability of branched glycerol dialkyl glycerol tetraethers (brGDGTs) in a  
687 temperate lake system, *Geochimica et Cosmochimica Acta*, 144, 173-187,  
688 10.1016/j.gca.2014.08.027, 2014.

689 Lu, H., Wu, N., Liu, K.-b., Zhu, L., Yang, X., Yao, T., Wang, L., Li, Q., Liu, X., Shen, C., Li,  
690 X., Tong, G., and Jiang, H.: Modern pollen distributions in Qinghai-Tibetan Plateau and the  
691 development of transfer functions for reconstructing Holocene environmental changes,  
692 *Quaternary Science Reviews*, 30, 947-966, 10.1016/j.quascirev.2011.01.008, 2011.

693 Ma, W., Li, G., Song, J., Yan, L., and Wu, L.: Effect of Vegetation Degradation on Soil  
694 Organic Carbon Pool and Carbon Pool Management Index in the Gahai Wetland, China, *Acta*  
695 *Agrestia Sinica*, 27, 687-694, 2019.

696 Marcott, S. A., Shakun, J. D., Clark, P. U., and Mix, A. C.: A Reconstruction of Regional and  
697 Global Temperature for the Past 11,300 Years, *Science*, 339, 1198-1201,  
698 10.1126/science.1228026, 2013.

699 Marsicek, J., Shuman, B. N., Bartlein, P. J., Shafer, S. L., and Brewer, S.: Reconciling  
700 divergent trends and millennial variations in Holocene temperatures, *Nature*, 554, 92-+,  
701 10.1038/nature25464, 2018.

702 Martin, C., Ménot, G., Thouveny, N., Peyron, O., Andrieu-Ponel, V., Montade, V., Davtian,  
703 N., Reille, M., and Bard, E.: Early Holocene Thermal Maximum recorded by branched

704 tetraethers and pollen in Western Europe (Massif Central, France), *Quaternary Science*  
705 *Reviews*, 228, 106109, 10.1016/j.quascirev.2019.106109, 2020.

706 Martínez-Sosa, P., Tierney, J. E., Stefanescu, I. C., Dearing Crampton-Flood, E., Shuman, B.  
707 N., and Routson, C.: A global Bayesian temperature calibration for lacustrine brGDGTs,  
708 *Geochimica et Cosmochimica Acta*, 305, 87-105, 10.1016/j.gca.2021.04.038, 2021.

709 Moser, K. A., Baron, J. S., Brahney, J., Oleksy, I. A., Saros, J. E., Hundey, E. J., Sadro, S.,  
710 Kopáček, J., Sommaruga, R., Kainz, M. J., Strecker, A. L., Chandra, S., Walters, D. M.,  
711 Preston, D. L., Michelutti, N., Lepori, F., Spaulding, S. A., Christianson, K. R., Melack, J. M.,  
712 and Smol, J. P.: Mountain lakes: Eyes on global environmental change, *Global and Planetary*  
713 *Change*, 178, 77-95, 10.1016/j.gloplacha.2019.04.001, 2019.

714 Opitz, S., Zhang, C., Herzschuh, U., and Mischke, S.: Climate variability on the south-eastern  
715 Tibetan Plateau since the Lateglacial based on a multiproxy approach from Lake Naleng –  
716 comparing pollen and non-pollen signals, *Quaternary Science Reviews*, 115, 112-122,  
717 10.1016/j.quascirev.2015.03.011, 2015.

718 Osman, M. B., Tierney, J. E., Zhu, J., Tardif, R., Hakim, G. J., King, J., and Poulsen, C. J.:  
719 Globally resolved surface temperatures since the Last Glacial Maximum, *Nature*, 599, 239-  
720 244, 10.1038/s41586-021-03984-4, 2021.

721 Pang, H., Hou, S., Zhang, W., Wu, S., Jenk, T. M., Schwikowski, M., and Jouzel, J.:  
722 Temperature Trends in the Northwestern Tibetan Plateau Constrained by Ice Core Water  
723 Isotopes Over the Past 7,000 Years, *Journal of Geophysical Research-Atmospheres*, 125,  
724 10.1029/2020jd032560, 2020.

725 Qiu, J.: The third pole, *Nature*, 454, 393-396, 10.1038/454393a, 2008.

726 Russell, J. M., Hopmans, E. C., Loomis, S. E., Liang, J., and Sinninghe Damsté, J. S.:  
727 Distributions of 5- and 6-methyl branched glycerol dialkyl glycerol tetraethers (brGDGTs) in  
728 East African lake sediment: Effects of temperature, pH, and new lacustrine paleotemperature  
729 calibrations, *Organic Geochemistry*, 117, 56-69, 10.1016/j.orggeochem.2017.12.003, 2018.

730 Sinninghe Damsté, J. S., Hopmans, E. C., Pancost, R. D., Schouten, S., and Geenevasen, J. A.  
731 J.: Newly discovered non-isoprenoid glycerol dialkyl glycerol tetraether lipids in sediments,  
732 *Chemical Communications*, 1683-1684, 10.1039/b004517i, 2000.

733 Sinninghe Damsté, J. S., Ossebaar, J., Abbas, B., Schouten, S., and Verschuren, D.: Fluxes  
734 and distribution of tetraether lipids in an equatorial African lake: Constraints on the  
735 application of the TEX86 palaeothermometer and BIT index in lacustrine settings,  
736 *Geochimica et Cosmochimica Acta*, 73, 4232-4249, 10.1016/j.gca.2009.04.022, 2009.

737 Sun, Q., Chu, G., Liu, M., Xie, M., Li, S., Ling, Y., Wang, X., Shi, L., Jia, G., and Lü, H.:  
738 Distributions and temperature dependence of branched glycerol dialkyl glycerol tetraethers in  
739 recent lacustrine sediments from China and Nepal, *Journal of Geophysical Research*, 116,  
740 10.1029/2010jg001365, 2011.

741 Sun, X., Zhao, C., Zhang, C., Feng, X., Yan, T., Yang, X., and Shen, J.: Seasonality in  
742 Holocene Temperature Reconstructions in Southwestern China, *Paleoceanography and*  
743 *Paleoclimatology*, 36, 10.1029/2020pa004025, 2021.

744 Sun, Z., Hou, X., Ji, K., Yuan, K., Li, C., Wang, M., and Hou, J.: Potential winter-season bias  
745 of annual temperature variations in monsoonal Tibetan Plateau since the last deglaciation,  
746 *Quaternary Science Reviews*, 292, 10.1016/j.quascirev.2022.107690, 2022.

747 Thompson, L. G., Yao, T., Davis, M. E., Henderson, K. A., MosleyThompson, E., Lin, P. N.,

748 Beer, J., Synal, H. A., ColeDai, J., and Bolzan, J. F.: Tropical climate instability: The last  
749 glacial cycle from a Qinghai-Tibetan ice core, *Science*, 276, 1821-1825,  
750 10.1126/science.276.5320.1821, 1997.

751 Tian, L., Wang, M., Zhang, X., Yang, X., Zong, Y., Jia, G., Zheng, Z., and Man, M.:  
752 Synchronous change of temperature and moisture over the past 50 ka in subtropical  
753 southwest China as indicated by biomarker records in a crater lake, *Quaternary Science*  
754 *Reviews*, 212, 121-134, 10.1016/j.quascirev.2019.04.003, 2019.

755 Tierney, J. E. and Russell, J. M.: Distributions of branched GDGTs in a tropical lake system:  
756 Implications for lacustrine application of the MBT/CBT paleoproxy, *Organic Geochemistry*,  
757 40, 1032-1036, 10.1016/j.orggeochem.2009.04.014, 2009.

758 Tierney, J. E., Russell, J. M., Eggermont, H., Hopmans, E. C., Verschuren, D., and Sinninghe  
759 Damsté, J. S.: Environmental controls on branched tetraether lipid distributions in tropical  
760 East African lake sediments, *Geochimica et Cosmochimica Acta*, 74, 4902-4918,  
761 10.1016/j.gca.2010.06.002, 2010.

762 Tierney, J. E., Zhu, J., King, J., Malevich, S. B., Hakim, G. J., and Poulsen, C. J.: Glacial  
763 cooling and climate sensitivity revisited, *Nature*, 584, 569+, 10.1038/s41586-020-2617-x,  
764 2020.

765 van Bree, L. G. J., Peterse, F., Baxter, A. J., De Crop, W., van Grinsven, S., Villanueva, L.,  
766 Verschuren, D., and Sinninghe Damsté, J. S.: Seasonal variability and sources of in situ  
767 brGDGT production in a permanently stratified African crater lake, *Biogeosciences*, 17,  
768 5443-5463, 10.5194/bg-17-5443-2020, 2020.

769 Wang, G., Wang, Y., Wei, Z., He, W., Ma, X., and Zhang, T.: Reconstruction of temperature  
770 and precipitation spanning the past 28 kyr based on branched tetraether lipids from Qionghai  
771 Lake, southwestern China, *Palaeogeography Palaeoclimatology Palaeoecology*, 562,  
772 10.1016/j.palaeo.2020.110094, 2021a.

773 Wang, H., An, Z., Lu, H., Zhao, Z., and Liu, W.: Calibrating bacterial tetraether distributions  
774 towards in situ soil temperature and application to a loess-paleosol sequence, *Quaternary*  
775 *Science Reviews*, 231, 10.1016/j.quascirev.2020.106172, 2020.

776 Wang, H., Chen, W., Zhao, H., Cao, Y., Hu, J., Zhao, Z., Cai, Z., Wu, S., Liu, Z., and Liu, W.:  
777 Biomarker-based quantitative constraints on maximal soil-derived brGDGTs in modern lake  
778 sediments, *Earth and Planetary Science Letters*, 602, 10.1016/j.epsl.2022.117947, 2023.

779 Wang, H., Liu, W., He, Y., Zhou, A., Zhao, H., Liu, H., Cao, Y., Hu, J., Meng, B., Jiang, J.,  
780 Kolpakova, M., Krivonogov, S., and Liu, Z.: Salinity-controlled isomerization of lacustrine  
781 brGDGTs impacts the associated MBT5ME' terrestrial temperature index, *Geochimica et*  
782 *Cosmochimica Acta*, 305, 33-48, 10.1016/j.gca.2021.05.004, 2021b.

783 Wang, M., Liang, J., Hou, J., and Hu, L.: Distribution of GDGTs in lake surface sediments on  
784 the Tibetan Plateau and its influencing factors, *Science China Earth Sciences*, 59, 961-974,  
785 10.1007/s11430-015-5214-3, 2016.

786 Wang, M. D., Hou, J. Z., Duan, Y. W., Chen, J. H., Li, X. M., He, Y., Lee, S. Y., and Chen, F.  
787 H.: Internal feedbacks forced Middle Holocene cooling on the Qinghai-Tibetan Plateau,  
788 *Boreas*, 10.1111/bor.12531, 2021c.

789 Wang, N., Liu, L., Hou, X., Zhang, Y., Wei, H., and Cao, X.: Palynological evidence reveals  
790 an arid early Holocene for the northeast Tibetan Plateau, *Climate of the Past*, 18, 2381-2399,  
791 10.5194/cp-18-2381-2022, 2022.

792 Weber, Y., De Jonge, C., Rijpstra, W. I. C., Hopmans, E. C., Stadnitskaia, A., Schubert, C. J.,  
793 Lehmann, M. F., Sinninghe Damsté, J. S., and Niemann, H.: Identification and carbon isotope  
794 composition of a novel branched GDGT isomer in lake sediments: Evidence for lacustrine  
795 branched GDGT production, *Geochimica et Cosmochimica Acta*, 154, 118-129,  
796 10.1016/j.gca.2015.01.032, 2015.

797 Weber, Y., Sinninghe Damste, J. S., Zopfi, J., De Jonge, C., Gilli, A., Schubert, C. J., Lepori,  
798 F., Lehmann, M. F., and Niemann, H.: Redox-dependent niche differentiation provides  
799 evidence for multiple bacterial sources of glycerol tetraether lipids in lakes, *Proc Natl Acad*  
800 *Sci U S A*, 115, 10926-10931, 10.1073/pnas.1805186115, 2018.

801 Weijers, J. W. H., Schouten, S., van den Donker, J. C., Hopmans, E. C., and Sinninghe  
802 Damsté, J. S.: Environmental controls on bacterial tetraether membrane lipid distribution in  
803 soils, *Geochimica et Cosmochimica Acta*, 71, 703-713, 10.1016/j.gca.2006.10.003, 2007.

804 Woltering, M., Werne, J. P., Kish, J. L., Hicks, R., Sinninghe Damsté, J. S., and Schouten, S.:  
805 Vertical and temporal variability in concentration and distribution of thaumarchaeotal  
806 tetraether lipids in Lake Superior and the implications for the application of the TEX86  
807 temperature proxy, *Geochimica et Cosmochimica Acta*, 87, 136-153,  
808 10.1016/j.gca.2012.03.024, 2012.

809 Wu, D., Chen, X., Lv, F., Brenner, M., Curtis, J., Zhou, A., Chen, J., Abbott, M., Yu, J., and  
810 Chen, F.: Decoupled early Holocene summer temperature and monsoon precipitation in  
811 southwest China, *Quaternary Science Reviews*, 193, 54-67, 10.1016/j.quascirev.2018.05.038,  
812 2018.

813 Wu, J., Yang, H., Pancost, R. D., Naafs, B. D. A., Qian, S., Dang, X., Sun, H., Pei, H., Wang,  
814 R., Zhao, S., and Xie, S.: Variations in dissolved O<sub>2</sub> in a Chinese lake drive changes in  
815 microbial communities and impact sedimentary GDGT distributions, *Chemical Geology*, 579,  
816 10.1016/j.chemgeo.2021.120348, 2021.

817 Yan, T., Zhao, C., Yan, H., Shi, G., Sun, X., Zhang, C., Feng, X., and Leng, C.: Elevational  
818 differences in Holocene thermal maximum revealed by quantitative temperature  
819 reconstructions at ~30° N on eastern Tibetan Plateau, *Palaeogeography, Palaeoclimatology,*  
820 *Palaeoecology*, 570, 110364, 10.1016/j.palaeo.2021.110364, 2021.

821 Yao, T., Bolch, T., Chen, D., Gao, J., Immerzeel, W., Piao, S., Su, F., Thompson, L., Wada, Y.,  
822 Wang, L., Wang, T., Wu, G., Xu, B., Yang, W., Zhang, G., and Zhao, P.: The imbalance of the  
823 Asian water tower, *Nature Reviews Earth & Environment*, 3, 618-632, 10.1038/s43017-022-  
824 00299-4, 2022.

825 Zhang, C., Zhao, C., Yu, S.-Y., Yang, X., Cheng, J., Zhang, X., Xue, B., Shen, J., and Chen, F.:  
826 Seasonal imprint of Holocene temperature reconstruction on the Tibetan Plateau, *Earth-*  
827 *Science Reviews*, 226, 103927, 10.1016/j.earscirev.2022.103927, 2022a.

828 Zhang, E., Chang, J., Shulmeister, J., Langdon, P., Sun, W., Cao, Y., Yang, X., and Shen, J.:  
829 Summer temperature fluctuations in Southwestern China during the end of the LGM and the  
830 last deglaciation, *Earth and Planetary Science Letters*, 509, 78-87, 10.1016/j.epsl.2018.12.024,  
831 2019a.

832 Zhang, E., Chang, J., Cao, Y., Sun, W., Shulmeister, J., Tang, H., Langdon, P. G., Yang, X.,  
833 and Shen, J.: Holocene high-resolution quantitative summer temperature reconstruction based  
834 on subfossil chironomids from the southeast margin of the Qinghai-Tibetan Plateau,  
835 *Quaternary Science Reviews*, 165, 1-12, 10.1016/j.quascirev.2017.04.008, 2017.

836 Zhang, G., Luo, W., Chen, W., and Zheng, G.: A robust but variable lake expansion on the  
837 Tibetan Plateau, *Science Bulletin*, 64, 1306-1309, 10.1016/j.scib.2019.07.018, 2019b.

838 Zhang, W., Wu, H., Cheng, J., Geng, J., Li, Q., Sun, Y., Yu, Y., Lu, H., and Guo, Z.: Holocene  
839 seasonal temperature evolution and spatial variability over the Northern Hemisphere  
840 landmass, *Nat Commun*, 13, 5334, 10.1038/s41467-022-33107-0, 2022b.

841 Zhao, B., Castaneda, I. S., Bradley, R. S., Salacup, J. M., de Wet, G. A., Daniels, W. C., and  
842 Schneider, T.: Development of an in situ branched GDGT calibration in Lake 578, southern  
843 Greenland, *Organic Geochemistry*, 152, 10.1016/j.orggeochem.2020.104168, 2021a.

844 Zhao, C., Liu, Z. H., Rohling, E. J., Yu, Z. C., Liu, W. G., He, Y. X., Zhao, Y., and Chen, F. H.:  
845 Holocene temperature fluctuations in the northern Tibetan Plateau, *Quaternary Research*, 80,  
846 55-65, 10.1016/j.yqres.2013.05.001, 2013.

847 Zhao, C., Rohling, E. J., Liu, Z., Yang, X., Zhang, E., Cheng, J., Liu, Z., An, Z., Yang, X.,  
848 Feng, X., Sun, X., Zhang, C., Yan, T., Long, H., Yan, H., Yu, Z., Liu, W., Yu, S.-Y., and Shen,  
849 J.: Possible obliquity-forced warmth in southern Asia during the last glacial stage, *Science*  
850 *Bulletin*, 66, 1136-1145, 10.1016/j.scib.2020.11.016, 2021b.

851 Zheng, Y., Li, Q., Wang, Z., Naafs, B. D. A., Yu, X., and Pancost, R. D.: Peatland GDGT  
852 records of Holocene climatic and biogeochemical responses to the Asian Monsoon, *Organic*  
853 *Geochemistry*, 87, 86-95, 10.1016/j.orggeochem.2015.07.012, 2015.

854 Zhou, W., Yu, S.-Y., Burr, G. S., Kukla, G. J., Jull, A. J. T., Xian, F., Xiao, J., Colman, S. M.,  
855 Yu, H., Liu, Z., and Kong, X.: Postglacial changes in the Asian summer monsoon system: a  
856 pollen record from the eastern margin of the Tibetan Plateau, *Boreas*, 39, 528-539,  
857 10.1111/j.1502-3885.2010.00150.x, 2010.

858 Zielinski, G. A. and Mershon, G. R.: Paleoenvironmental implications of the insoluble  
859 microparticle record in the GISP2 (Greenland) ice core during the rapidly changing climate  
860 of the Pleistocene-Holocene transition, *Geological Society of America Bulletin*, 109, 547-559,  
861 10.1130/0016-7606(1997)109<0547:piotim>2.3.co;2, 1997.

862

863